



Mixed Signals: interpreting mixing patterns of different soil bioturbation processes through luminescence and numerical modelling

W. Marijn van der Meij¹, Svenja Riedesel^{1,2}, and Tony Reimann¹

¹Institute of Geography, University of Cologne, Zùlpicher StraÙe 45, 50674 Cologne, Germany

²Department of Physics, Technical University of Denmark, Frederiksborgvej 399, 4000 Roskilde, Denmark

Correspondence: W. Marijn van der Meij (m.vandermeij@uni-koeln.de)

Received: 16 May 2024 – Discussion started: 22 May 2024

Revised: 24 September 2024 – Accepted: 4 November 2024 – Published: 14 January 2025

Abstract. Soil bioturbation plays a key role in soil functions such as carbon and nutrient cycling. Despite its importance, fundamental knowledge on how different organisms and processes impact the rates and patterns of soil mixing during bioturbation is lacking. However, this information is essential for understanding the effects of bioturbation in present-day soil functions and on long-term soil evolution.

Luminescence, a light-sensitive mineral property, serves as a valuable tracer for long-term soil bioturbation over decadal to millennial timescales. The luminescence signal resets (bleaches) when a soil particle is exposed to daylight at the soil surface and accumulates when the particle is buried in the soil, acting as a proxy for subsurface residence times. In this study, we compiled three luminescence datasets of soil mixing by different biota and compared them to numerical simulations of bioturbation using the ChronoLorica soil-landscape evolution model. The goal was to understand how different mixing processes affect depth profiles of luminescence-based metrics, such as the modal age, width of the age distributions and fraction of the bleached particles.

We focus on two main bioturbation processes: mounding (advective transport of soil material to the surface) and subsurface mixing (diffusive subsurface transport). Each process has a distinct effect on the luminescence metrics, which we summarized in a conceptual diagram to help with qualitative interpretation of luminescence-based depth profiles. A first attempt to derive quantitative information from luminescence datasets through model calibration showed promising results but also highlighted gaps in the data that must be addressed before accurate, quantitative estimates of bioturbation rates and processes are possible.

The new numerical formulations of bioturbation, which are provided in an accompanying modelling tool, provide new possibilities for calibration and more accurate simulation of the processes in soil function and soil evolution models.

1 Introduction

Bioturbation is the umbrella term for soil mixing processes by various organisms. Bioturbation plays a key role in soil nutrient cycling, carbon sequestration, erosion and the re-distribution of contaminants and pollutants (Wilkinson et al., 2009; Briones, 2014; Creamer et al., 2022). Despite its pivotal role in regulating soil functions, we have an incomplete understanding regarding how different organisms and ecosystems impact the types and rates of mixing processes,

how these rates vary with soil depth and how different mixing processes interact within the soil (Schiffers et al., 2011; Michel et al., 2022). These insights are essential for accurately modelling the effects of bioturbation on present-day soil functions and the long-term evolution of soils (Creamer et al., 2022; Meng et al., 2022).

In this work, we examine two key soil bioturbation processes: mounding and subsurface mixing (Wilkinson et al., 2009). *Mounding* is the upward advective transport of soil material, which is deposited on the surface in mounds

and later eroded and buried by newly mounded material. *Subsurface mixing* involves the diffusive upward and downward exchange of soil material throughout the entire soil profile at various depths. Many soil organisms display both processes in different capacities, depending on their feeding and burrowing behaviour. Gophers and mound-building termites such as *Macrotermes* are mainly known for mounding (Gabet, 2000; Kristensen et al., 2015), while organisms that mainly reside in the subsurface, such as gallery-building ants, endogeic earthworms and tree roots, typically show subsurface mixing behaviour (Richards, 2009; Halfen and Hasiotis, 2010; Taylor et al., 2019). Anecic earthworms and *Aphaenogaster* ants, which visit the surface and create deep vertical burrows and galleries, contribute to both mounding and subsurface mixing (Bouché, 1977; Richards, 2009). Bioturbation is thus often an interplay of mounding and subsurface mixing driven by various organisms but also by environmental and climatic factors (Wilkinson et al., 2009; Kraus et al., 2022), which leads to mixed bioturbation signals in the soil. Although subsurface mixing is generally considered the dominant process, there is a lack of data or methods to differentiate the effects of both bioturbation processes (Wilkinson et al., 2009; Halfen and Hasiotis, 2010; Michel et al., 2022).

Luminescence emitted by quartz and feldspar grains has been used successfully as a tracer for bioturbation (Heimsath et al., 2002; Madsen et al., 2011; Stockmann et al., 2013; Johnson et al., 2014; Gliganic et al., 2015; Hanson et al., 2015; Reimann et al., 2017; Román-Sánchez et al., 2019b; Zhang et al., 2024). The luminescence signal accumulates over time due to ionizing radiation coming from naturally occurring radionuclides in the soil (uranium and thorium decay chains and potassium-40) and from cosmic rays. The luminescence signal is reset (bleached) when a soil particle is exposed to daylight. Thus, the luminescence signal is a proxy for the residence time of soil particles in the subsurface and is ideally measured on single grains when used as a tracer for soil mixing (Duller, 2008). The distribution of the luminescence signal of different grains in a sample informs us about the type and intensity of the mixing process (Bateman et al., 2003, 2007). Moreover, their changes with depth provide additional information on the rates, patterns and intensity of the bioturbation.

Luminescence signals are often used in combination with numerical or analytical tools to calculate particle ages and soil mixing rates and to characterize mixing patterns (Furbish et al., 2018a, b; Román-Sánchez et al., 2019a; Schiffers et al., 2011; Gray et al., 2020; Yates et al., 2024). These tools are often based on a single diffusion-based implementation of the mixing process, which limits the possibilities of separating mixing signals by different biota (Schiffers et al., 2011), or are based on models stemming from aquatic ecology without adequate testing for terrestrial environments (Michel et al., 2022). Recent developments in soil-landscape evolution modelling enable the integration of luminescence tracers with process-based simulations of soil and landscape

processes (ChronoLorica model; Van der Meij et al., 2023). This integration enables the simulation of the effects of different bioturbation processes on luminescence–depth profiles, which can help to quantify the impacts of different bioturbation processes on soil mixing, better formulate bioturbation processes and their effects on nutrient cycling and other soil functions (Creamer et al., 2022), simulate soil mixing over different spatial and temporal scales (e.g. Schiffers et al., 2011) and better represent the role of biota in soil-landscape evolution models (Meng et al., 2022).

The objective of this study is to provide qualitative and quantitative tools to differentiate the impacts of mounding and subsurface mixing during soil bioturbation using luminescence tracers. By integrating experimental luminescence-based bioturbation datasets with soil evolution modelling, we aim to (1) characterize typical luminescence–depth profiles for mounding and subsurface mixing, (2) determine how varying parameters and combinations of these processes affect these depth profiles and (3) derive quantitative process rates and contributions from experimental data through model calibration.

2 Methods

2.1 Conceptual models of soil mixing

Mounding and subsurface mixing have distinct effects on the soil and luminescence tracers. In this section, we conceptually discuss these effects as a basis for their numerical implementation.

Soil bioturbation by mounding causes a net upward transport of soil material to the soil surface (Fig. 1a). This soil material is mined from previously buried material from the upper part of the soil (~ 1 m for termites; Kristensen et al., 2015), effectively leading to recycling of soil material in the mounding process over longer timescales. This recycling exposes a large part of the soil grains to daylight, leading to only a limited amount of non-surfaced grains that can carry a saturated luminescence signal. Typical mounding organisms are gophers, moles and termites (Gabet, 2000; Wilkinson et al., 2009; Kristensen et al., 2015). Mounding rates most likely decrease with depth due to decreasing biotic activity (Gray et al., 2020).

The diffusion-like transport caused by organisms that perform subsurface mixing moves soil material in between subsurface layers (Fig. 1b). Typical mixing organisms are endogeic and anecic earthworms which (partly) live underground (Taylor et al., 2019), ants and subterranean termites that create subsurface galleries (Richards, 2009; Halfen and Hasiotis, 2010; Rink et al., 2013; Stewart and Anand, 2014; Taylor et al., 2019) and tree roots which shift material around when growing and which leave pores that can be filled with material after decay of the root material (Johnson et al., 2014; Ruiz et al., 2015). With subsurface mixing, there is a much smaller proportion of grains that are transported to the sur-

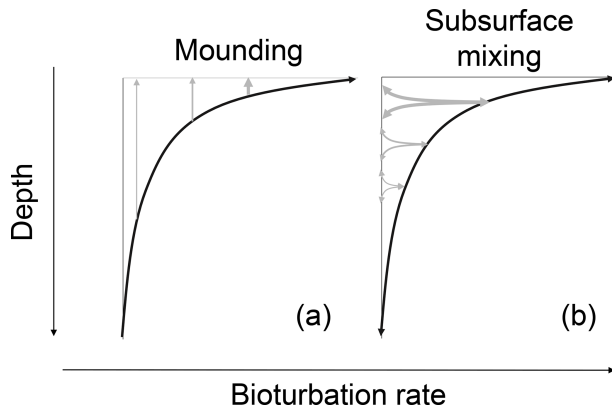


Figure 1. Conceptual drawing of (a) mounding and (b) subsurface mixing. Subsurface mixing and mounding are visualized here with an exponential depth function (see Sect. 2.3.2). The arrows indicate direction and their thickness the intensity of soil transport.

face, leaving a higher proportion of non-surfaced grains. Also, for subsurface mixing, mixing rates likely decrease with depth due to decreased biotic activity (Fig. 1b).

2.2 Experimental studies

We compiled three quartz and feldspar single-grain luminescence datasets of soil mixing by different organisms to characterize luminescence–depth profiles (Table 1). The main bioturbating organisms are termites that preferentially mound (Kristensen et al., 2015), anecic earthworms that both mound and mix the subsurface (von Suchodoletz et al., 2023) and ants that mainly mix the subsurface (Román-Sánchez et al., 2019b). All measurements were performed using Risø TL/OSL DA15 and DA20 luminescence readers equipped with $^{90}\text{Sr}/^{90}\text{Y}$ beta sources. The luminescence signals of single-grain quartz for the termite study were stimulated using a green laser for single grains (Kristensen et al., 2015). The signals were detected by a UV-sensitive photomultiplier tube (PMT) through a 7.5 mm Schott U-340 filter. K-rich feldspars were stimulated using an IR laser and the signals were detected with a LOT/ORIEL D410 interference filter (Román-Sánchez et al., 2019b; von Suchodoletz et al., 2023). Details regarding the sample preparation and the exact measurement conditions are given in the respective publications and a summary is provided in Table 1.

From these datasets, we are only interested in the ages of grains that have been bioturbated by the current dominant bioturbating agent. For the termite and worm datasets, there is a defined time period in which the current agent has been and continues to be active (Table 1). Grains falling outside of this time frame are filtered out and excluded from our analysis of age distributions. Instead, we incorporate this fraction of particles (f_{filtered}) with the fraction of grains that have not reached the surface at all and have a saturated luminescence signal ($f_{\text{non-surfaced}}$). The remaining fraction (f_{bio}) contains

the grains that have reached the surface through bioturbation by the current dominant agent (Eq. 1). f_{bio} , or the bioturbated fraction, is similar to the non-saturation factor (NSF) as defined by Reimann et al. (2017), with the addition of another rejection criterion based on the bioturbation period.

$$f_{\text{bio}} = 1 - (f_{\text{non-surfaced}} + f_{\text{filtered}}) \quad (1)$$

2.3 Simulations

2.3.1 Model description

The bioturbation simulations are performed using the ChronoLorica model (Van der Meij and Temme, 2022; Van der Meij et al., 2023), which is an extension of the Lorica soil-landscape evolution model (Temme and Vanwallegem, 2016; Van der Meij et al., 2020). Lorica is a mass-based four-dimensional numerical model that simulates the development of terrain and soil properties due to various geomorphic and pedogenic processes. The landscape is represented by a raster, where every raster cell contains a predefined number of soil layers. The layers contain a mass of five mineral soil textures (coarse, sand, silt, clay and fine clay) and two organic matter types (young and old). Throughout the simulations, the contents of the layers change due to the addition, removal or transformation of the soil material by the simulated processes. At this stage, the model is insensitive to parent material variations, as it does not include grain-size-dependent mixing rates. Changes in the mass composition of each layer are translated into changes in layer thickness and surface elevation through the bulk density. Lorica works with dynamic layer thicknesses, enabling easy calculation of additions and subtractions from each layer. The layers start with a predefined initial thickness. When a layer thickness becomes more than 55 % thicker than the initial thickness, the layer splits into two new layers. When a layer thickness becomes thinner than 55 % of the initial thickness, the layer is merged with a neighbouring layer. Due to its coarse spatial resolution and temporal resolution, the model is not suitable for simulating pore size dynamics due to bioturbation.

The ChronoLorica extension couples the pedogenic and geomorphic processes in the model to several geochronometers. In this study, we use soil particle burial ages, akin to luminescent grains, as tracers for bioturbation. We term these *luminescence particles* in this study. These particles do not have specific dimensions but should be considered objects that have a specific age that is analogous to a luminescence age. This age increases during their time of burial and resets when the particles are transported into the surface layer. This surface layer has a fixed depth that represents the bleaching depth. The transport of luminescence particles is coupled to the transport of the sand fraction of the model, because the sand fraction is the texture class that is typically used for single-grain luminescence dating (Duller, 2008). Due to memory constraints in the model, the number of tracked luminescence particle ages is much lower than the number of

Table 1. Overview of the experimental single-grain luminescence datasets used in this study. When reported in the original publications, species names, climate zones and ecosystems are mentioned. Q: quartz; FSP: feldspar; SG: single grain; post-IR IRSL: post-infrared infrared-stimulated luminescence; PH: preheat.

Organism	Primary mixing process	Climate zone and ecosystem	Reference	Selected profile	Active mixing depth	Defined bioturbation period or saturation criteria	Luminescence method
Termites (<i>Macrotermes natalensis</i>)	Mounding	Tropical (Aw), savannah	Kristensen et al. (2015)	Unit II	1.02 m	< 4 ka, onset of deforestation and start of savannah ecosystem	Q SG, OSL, grain size 90–180 μm
Anecic earthworms	Subsurface mixing and mounding	Warm-summer humid continental (Dfb), ecosystem not reported	von Suchodoletz et al. (2023)	Profile 2	60 cm	< 13.2 ka, estimated start of bioturbation by earthworms > 3.8 ka, end of bioturbation due to burial of soil below burial mound	FSP SG, post-IR ₅₀ IRSL ₁₅₀ (PH 175 °C, 60 s), grain size 212–250 μm
Ants	Subsurface mixing	Mediterranean (BSk), oak-woodland savannah	Román-Sánchez et al. (2019b)	SC-10	50 cm	2* D_0 (Wintle and Murray, 2006)	FSP SG, post-IR ₅₀ IRSL ₁₇₅ g (PH 200 °C, 60 s), grain size 212–250 μm

sand particles present in each layer. Therefore, we used a probabilistic approach to determine whether a luminescence particle is transported together with the sand from one layer to another. The transport probability for each individual particle is determined by dividing the transported mass of sand out of a source layer by the total mass of sand present in that source layer (Eq. 2).

$$P_{\text{transport}} = \frac{\text{sand transported [kg]}}{\text{total sand present [kg]}} \quad (2)$$

2.3.2 Depth functions

Bioturbation is most likely a depth-dependent process, but whether the mixing rates decrease linearly or exponentially with depth is still unknown (Gray et al., 2020). In our simulations, we consider three typical depth functions that describe how mixing intensity changes with increasing soil depth (Minasny et al., 2016; Fig. 2). These depth functions can be applied to both bioturbation processes. The depth functions describe (i) a linear decrease with depth (*gradational*, $df_{\text{grd}}(z)$; Eq. 3), (ii) an exponential decrease with depth (*exponential*, $df_{\text{exp}}(z)$; Eq. 4) and (iii) a uniform mixing rate, which reduces abruptly to zero below the mixing zone (*abrupt*, $df_{\text{abr}}(z)$; Eq. 5). The depth decay parameters (dd_{grd} , dd_{exp} and dd_{abr}) [m^{-1}] determine the shape and gradient of the depth functions.

$$df_{\text{grd}}(z) = \begin{cases} -dd_{\text{grd}} \times z, & z \leq \frac{1}{dd_{\text{grd}}} \\ 0, & z > \frac{1}{dd_{\text{grd}}} \end{cases} \quad (3)$$

$$df_{\text{exp}}(z) = 1 - e^{-dd_{\text{exp}} \times z} \quad (4)$$

$$df_{\text{abr}}(z) = \begin{cases} 1, & z \leq dd_{\text{abr}} \\ 0, & z > dd_{\text{abr}} \end{cases} \quad (5)$$

The total bioturbation occurring in the soil profile, BT_{pot} [$\text{kg m}^{-2} \text{a}^{-1}$], is distributed across all the soil layers using one of the depth functions (Eqs. 3–5) and the depths of each layer (Eq. 6). To determine how much bioturbation occurs in a particular layer, the depth function $df(z)$ is integrated between the upper and lower depths of that layer (z_{upper} and z_{lower}). This value is divided by the integral of the depth function $df(z)$ over the entire active mixing depth. The resulting fraction is multiplied by BT_{pot} to calculate the bioturbation occurring in that specific layer (BT_{layer} , $\text{kg m}^{-2} \text{a}^{-1}$). The limit of the active mixing depth is indicated by the parameter z_{lim} , which is $1/dd_{\text{grd}}$ for the gradational function, the total soil depth sd for the exponential function (where $z \leq sd$), and dd_{abr} for the abrupt function.

$$BT_{\text{layer}} = BT_{\text{pot}} \times \frac{\int_{z_{\text{upper}}}^{z_{\text{lower}}} df(z) dz}{\int_0^{z_{\text{lim}}} df(z) dz} \quad (6)$$

2.3.3 Process descriptions

We simulate the mounding process as upward transport of soil material from the subsurface. Equation (6) determines how much material is taken from each soil layer. This material is then transported to the surface layer, gradually burying previously mounded material. In this implementation, the development and erosion of surface mounds are simplified into generation of a new surface layer that results from the mound erosion.

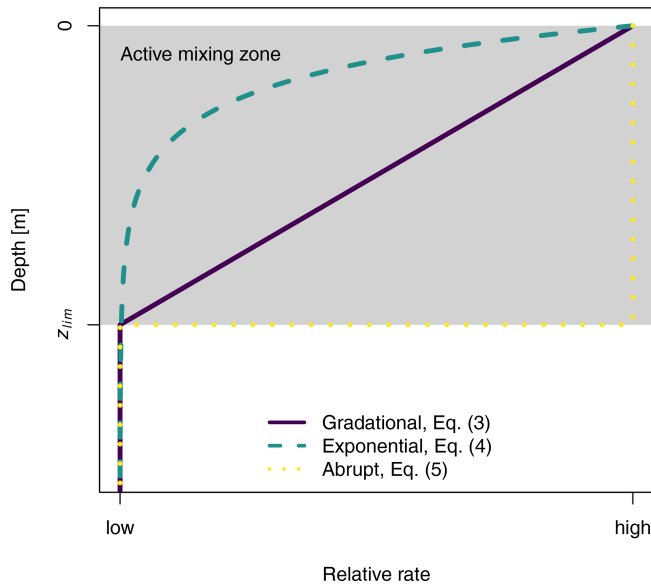


Figure 2. Depth functions that are used for bioturbation simulations. The depth functions determine how bioturbation rates change with soil depth. The parameters are selected so that all bioturbation effectively occurs in the active mixing zone (grey area), ranging from the surface to the depth of z_{lim} .

The subsurface mixing process is simulated by an exchange of soil material between all present soil layers (Fig. 1b). Equation (6) determines how much material each soil layer (donor layer) can exchange in total with all other exchange layers in the profile. The exchange $BT_{exchange}$ between the donor layer and the exchange layers is controlled by Eq. (7). This equation is similar to Eq. (6) in that it calculates the proportion of material exchange by bioturbation for a certain donor layer by integrating and dividing exponential depth functions. Equation (7) integrates an exponential equation over the vertical distance from the centre depth of the donor layer (z_{layer}) to the upper and lower depths of an exchange layer (z_{upper} and z_{lower}). This integral is divided by the sum of the integrals of two other exponential equations, starting from z_{layer} and going towards the soil surface ($z = 0$) and towards the bottom of the soil profile (sd). Through this equation, the amount of exchange between a donor layer and an exchange layer decreases with increasing distance between the layers, leading to diffusive mixing. The gradient of these exponential equations is controlled by the depth parameter $dd_{mix} [m^{-1}]$.

$$\begin{aligned}
 & BT_{exchange} = BT_{layer} \\
 & \times \frac{\left| \int_{z_{layer}-z_{upp}}^{z_{layer}-z_{lower}} e^{(-dd_{mix} \times z)} dz \right|}{\int_0^{sd-z_{layer}} e^{(-dd_{mix} \times z)} dz + \int_0^{z_{layer}} e^{(-dd_{mix} \times z)} dz} \quad (7)
 \end{aligned}$$

2.3.4 Model set-up

The model requires several parameters as input. These parameters can be grouped as environmental parameters that are determined by the organisms, ecosystem and climate (type of mixing processes, depth of active mixing zone and bioturbation period), model-based parameters that determine the configuration and construction of the modelled soil (soil and layer properties and bleaching depth) and process-based parameters that control process behaviour (bioturbation rate, depth functions and their parameters as well as a combination of processes). We ran our simulations using the values in Table 2 to illustrate how bioturbation affects luminescence-based depth profiles. These parameters should be constrained with experimental data or through inverse modelling when applied to real-world settings.

The environmental and model-based parameters were the same for all the simulations. We ran our simulations in a one-dimensional soil profile (pedon) to focus on vertical mixing processes and avoid effects from lateral redistribution processes. We simulated bioturbation over a period of 10 ka with an annual time step and a 1 m deep mixing zone. Due to the diffusive transport of subsurface mixing, material sourced in the active mixing zone can also be transported to layers below the active mixing zone. To account for this effect, we perform the simulations on a 2 m deep pedon. The pedon contains 200 soil layers 1 cm thick, with an upper layer of 5 mm representing the bleaching depth. The bleaching depth is based on model-based estimates (Furbish et al., 2018b) and is in line with light penetration depths in rocks (0–15 mm; Meyer et al., 2018). Each layer initially contains 150 luminescence particles. We simulate a uniform loess-like soil texture (25 % sand, 60 % silt and 15 % clay) with a constant bulk density of 1500 kg m^{-3} to avoid effects of textural and density variations on the age distributions in the simulations.

To study how the different processes and their parameters can influence luminescence-based depth profiles, we adjusted the process-based parameters in turns according to the values reported in Table 2 under “Scenario variations”. The standard total bioturbation BT_{pot} was set to $10 \text{ kg m}^{-2} \text{ a}^{-1}$ (loosely based on rates reported in Wilkinson et al., 2009: $0.3\text{--}110 \text{ kg m}^{-2} \text{ a}^{-1}$) and was varied from 1 to $10 \text{ kg m}^{-2} \text{ a}^{-1}$. The standard depth function was gradational but also varied with exponential and abrupt depth profiles. The depth parameters were selected such that the active mixing zone was restricted to the upper 1 m of the pedon to facilitate comparison between the simulations (Fig. 2). The two bioturbation processes were combined with various contributions ranging from 0 % to 100 %.

2.4 Data presentation and comparison

The model produces a large amount of data, as there are multiple simulations with a large number of layers that all contain about 150 luminescence particles. To facilitate visualiza-

Table 2. The parameters used in this study, categorized by type. The reported values remained constant throughout the simulations, except when adjusted according to the scenario variations listed in the last column.

Parameter type	Description	Value	Scenario variations
Environmental	Process	Mounding, subsurface mixing	
	Depth mixing zone	1	
	Bioturbation period [ka]	10	
Model-based	Soil depth [m]	2	
	Number of layers	200	
	Initial layer thickness [m]	0.01	
	Number of grains per layer	150	
	Bleaching depth [m]	0.005	
	Soil texture [% sand, silt and clay]	25, 60, 15	
	Bulk density [kg m^{-3}]	1500	
Process-based	Total bioturbation BT_{pot} [$\text{kg m}^{-2} \text{a}^{-1}$]	10	1–10
	Depth function df with depth parameter dd [m^{-1}] in brackets	Gradational (1)	Gradational (1), exponential (6), abrupt (1)
	Exchange parameter dd_{mix} [m^{-1}]	10	
	Relative contributions of processes [%]	100	0–100

tion and comparison between the different model scenarios, we took two steps to summarize the model output before presentation. First, we aggregated the model output by five layers so that their thickness resembles typical 5 cm thick OSL samples. This reduced the scatter resulting from the stochastic particle transport. Second, we presented the simulated ages as age distributions using probability functions (Bateman et al., 2003), which we then summarized with different metrics. Working with age distributions instead of statistical age models (e.g. Galbraith and Roberts, 2012) provides the advantage that we do not need to select a suitable age model and estimate its corresponding statistical parameters for each individual sample. This allows us to automate and speed up the modelling and calibration process (see Sect. 4.3) without introducing uncertainties from age model selection. One disadvantage of this approach is that we do not get a robust estimate of the error of the estimated age, but that is not required in this study. Because we expect non-normal or even multi-modal distributions in the data, we calculated the probability functions using a bandwidth following the method of Sheather and Jones (1991), which was developed for non-normal distributions. Saturated or non-bleached grains were excluded from the probability functions. We use the following metrics to summarize the age distributions:

- the modal age, which corresponds to the highest peak in the age distribution, which we consider the most likely burial age of the sample or layer;

- the interquartile range as a robust measure of the width of the distribution; and
- the bioturbated fraction (f_{bio} ; Eq. 1) as a measure of the fraction of bleached particles due to bioturbation.

Detailed plots of the simulated age distributions are provided in Figs. S1–S3 in the Supplement.

For the comparison of the experimental data and simulations, we normalized the depths and luminescence ages. For the experimental data, we normalized the depths by dividing the sampling depth by the maximum sampling depth and the luminescence ages by dividing the individual grain ages by the extent of the bioturbation period or the saturation criteria (Table 1). For the simulations, the depth was normalized by dividing the simulation depth by the active mixing depth of 1 m. The simulated ages were normalized by dividing by the simulation time of 10 ka.

3 Results

3.1 Experimental studies

Figure 3 shows the luminescence-based depth profiles from the experimental datasets. The plots are in order of increasing contribution of subsurface mixing (termites → worms → ants). With a larger contribution of subsurface mixing, the bioturbated fractions in the subsurface decrease. The termite and worm datasets show clear age–

depth trends, while the ant dataset shows a more scattered depth profile with a discontinuity in the modes. The termite and ant datasets show an increasing interquartile range with depth, while the worm dataset shows a relatively constant interquartile range. There are also clear differences in the bioturbated fraction. The termite dataset has a bioturbated fraction of over 50 % for the entire profile, with over 90 % bleaching in the upper 60 cm. The worm dataset also has well-bleached upper samples, but the bioturbated fraction approaches 25 % for the lowest sample. For the ants, only the upper sample shows good bleaching, with a bioturbated fraction of 97 %. This drops to 12 % and 6 % deeper in the profile, where only six to eight grains contain a luminescence signal.

3.2 Comparison of depth functions and bioturbation rates

The simulations of separate mounding and subsurface mixing processes with varying depth functions show clear differences in the resulting depth profiles (Fig. 4). The mounding shows curved age–depth trends with low interquartile ranges for all the different depth functions, which slightly increase closer to the lower boundary of the active mixing zone of 1 m (Fig. 4a). The gradational and exponential profiles approach the simulation time of 10 ka at the bottom of the profile, while the abrupt profile has much younger ages and a steeper depth profile. For each depth profile, almost all the particles have been bioturbated and bleached in the active mixing zone, as shown by the bioturbated fraction. Below this zone, none of the particles is bioturbated.

In contrast, the simulations of subsurface mixing show more chaotic, heterogeneous depth profiles of modal age that only show a general increasing trend with depth (Fig. 4b). The scatter in the depth trends of the modal ages also increases with depth and even reaches below the active mixing zone of 1 m due to exchange of material from bioturbated layers with all other soil layers. It should be noted that below 1 m there are only a few bioturbated grains present. The modes are similar for each simulated depth function, with slightly lower interquartile ranges for the upper part of the exponential depth profile. The interquartile ranges are high for all the simulations and generally decrease down the profile. This only concerns a small number of particles, as evidenced by the bioturbated fraction. The number of bioturbated particles decreases with the soil depth. The exponential profile contains the most bioturbated particles, followed by the gradational and abrupt profiles.

Variations in the bioturbation rate for the mounding and subsurface mixing processes show a clear effect on the steepness of the age–depth curves (Fig. 5). For the mounding process, higher rates lead to a steeper age–depth profile. Throughout the bioturbated profiles, almost all the luminescence particles have been bleached, independent of the rate. For the subsurface mixing process, higher rates show younger modal ages and higher bioturbated fractions. The

interquartile ranges show comparable trends, with different levels of scatter in the depth trends. Bioturbation rates also affect the depths of the mixed profiles, where lower bioturbation rates lead to shallower mixing bioturbated profiles.

3.3 Combination of mounding and subsurface mixing

Simulations where mounding and mixing were combined in different ratios show that the mounding process dominates the age–depth characteristics (Fig. 6a). Only when the fraction of mounding decreases to less than 5 % do the depth curves start to resemble the profile with solely subsurface mixing. The same pattern is visible for the bioturbated fraction, but the interquartile range reacts more quickly to changes in the ratio of mounding and subsurface mixing. Overall, a larger contribution of subsurface mixing leads to older luminescence particles in the profile (Fig. 6a), wider age distributions (Fig. 6b) and fewer bioturbated particles (Fig. 6c).

The general trends in the experimental data conform to the trends in the simulation data. Termites, as mounding organisms, show lower modes of ages compared to worms, which both mound and mix (Fig. 6a). The patterns in the topsoil are similar for all the simulations and experimental datasets, but in the subsurface the termites, as mounding organisms, show lower modes of ages compared to worms, which both mound and mix (Fig. 6a). The ant dataset shows lower modal ages than both of the other organisms. This can be attributed to the normalization procedure: while the observed period of bioturbation had been constrained in the cases of the termite and worm datasets, the ant dataset had no such constraint and was consequently normalized by much higher age values, leading to lower normalized ages (Table 1). The worm dataset shows higher interquartile ranges compared to the termite dataset (Fig. 6b). Also in this case, the ant dataset forms the exception due to the high normalization age. The simulated interquartile ranges are much lower for mounding-dominated scenarios than the experimental studies, indicating an underestimation of the spread in the age distributions. The bioturbated fraction also shows clear differences between mounding and subsurface mixing organisms, with a higher proportion of bioturbated grains for mounding organisms and mounding simulations (Fig. 6c).

4 Discussion

4.1 Mixing patterns by mounding and subsurface mixing

Bioturbation induces different mixing patterns in the soil, depending on the organism and process. Through the integration of luminescence tracers and numerical simulations, we identified distinct ways in which different processes and parameters impact soil mixing. Here, we will elaborate on the processes and their effects on luminescence tracers and show that they are consistent across the experimental datasets.

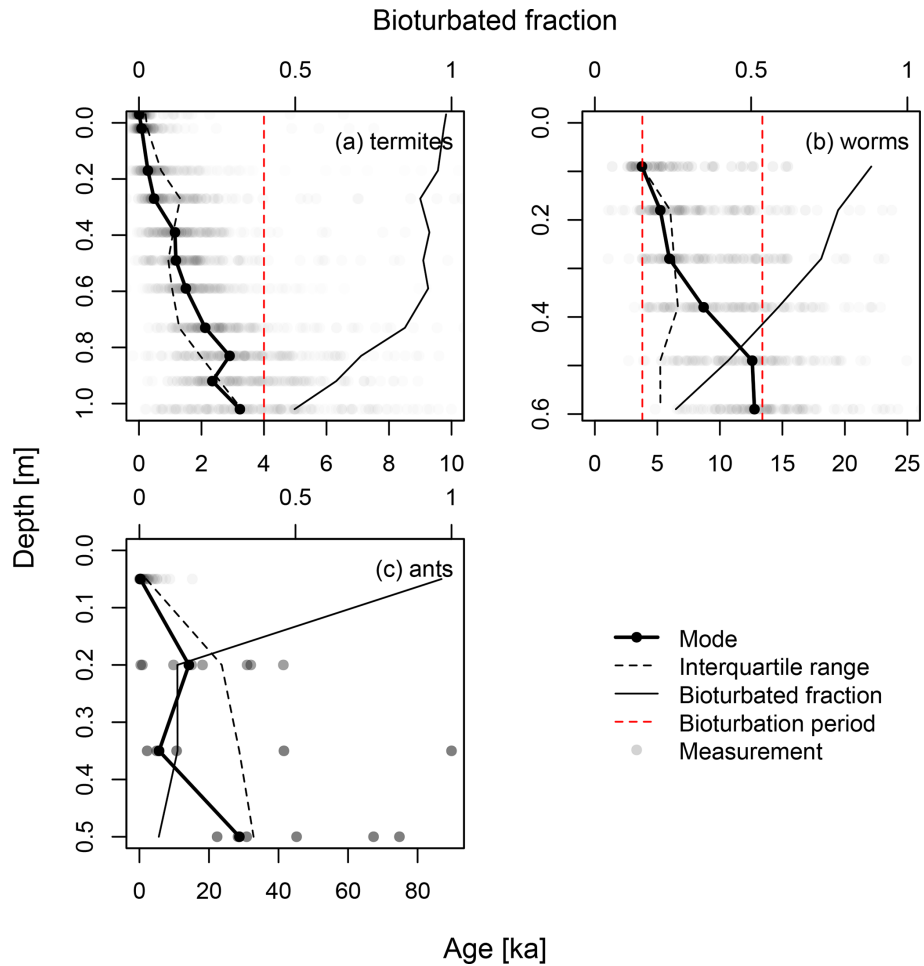


Figure 3. Age–depth profiles for the experimental datasets used in this study: **(a)** termites (Kristensen et al., 2015), **(b)** anecic earthworms (von Suchodoletz et al., 2023) and **(c)** ants (Román-Sánchez et al., 2019b). The bottom axes show the ages of the measurements. The upper axes show the bioturbated fraction. Where provided, the red dashed line indicates the period of bioturbation by the current agent (Table 1).

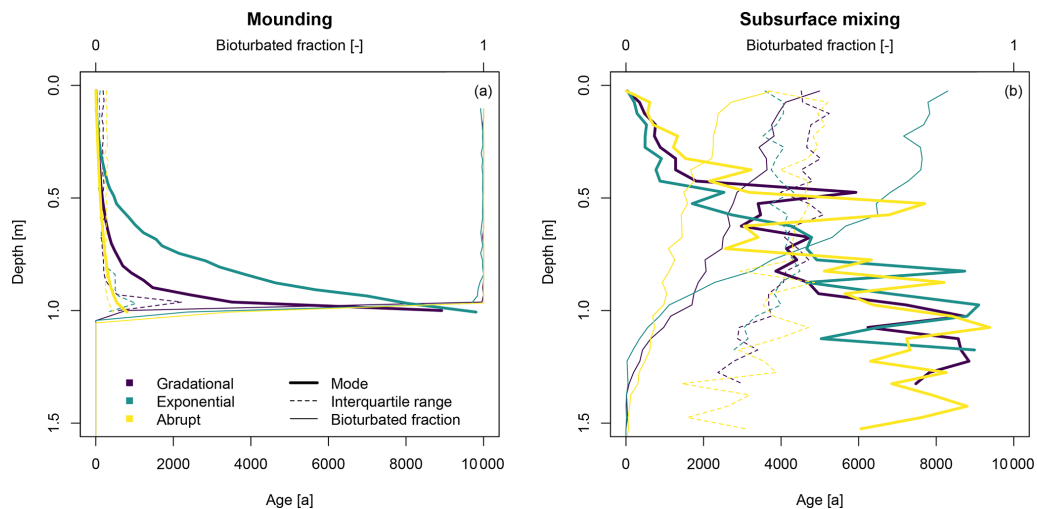


Figure 4. Luminescence-based depth profiles resulting from simulations of **(a)** mounding and **(b)** subsurface mixing, using different depth functions, with potential bioturbation rates of $10 \text{ kg m}^{-2} \text{ a}^{-1}$. Detailed plots of the simulated luminescence ages and their distributions are provided in Fig. S1.

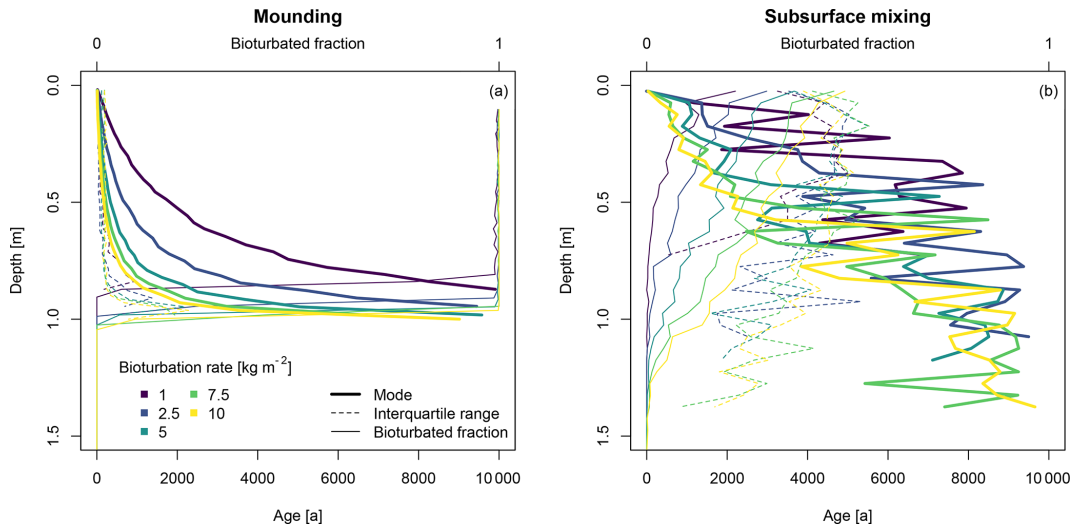


Figure 5. Age–depth profiles resulting from bioturbation by (a) mounding and (b) subsurface mixing, using a gradational depth profile and varying bioturbation rates. Detailed plots of the simulated luminescence ages and their distributions are provided in Fig. S2.

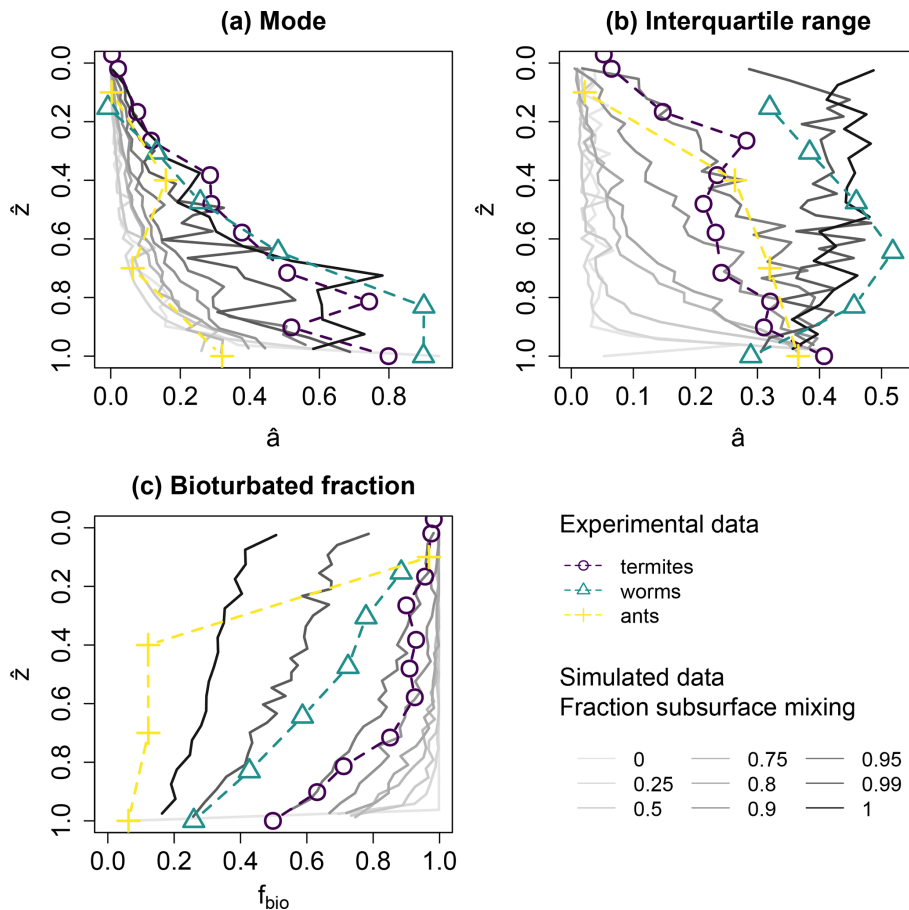


Figure 6. Statistics for mixes between mounding and subsurface mixing (grey lines), aggregated for five soil layers (~ 5 cm), compared to the experimental datasets (coloured lines and points). Results were normalized for age (\hat{a}) and depth (\hat{z}). The different windows show different statistics: (a) mode of age distributions, (b) interquartile range and (c) bioturbated fraction f_{bio} . The simulations were run with a gradational depth function, an active mixing zone of 1 m and a total bioturbation rate of $10 \text{ kg m}^{-2} \text{ a}^{-1}$, divided over the two processes. Detailed plots of the simulated luminescence ages and their distributions in this plot are provided in Fig. S3.

The upward advective transport of soil material by mounding animals continuously buries previously mounded material, which leads to age–depth profiles in the active mixing zone that resemble depositional profiles. The continuous upward transport of material to the surface results in a high degree of bleaching and consequently narrow age distributions, as evidenced by the termite dataset and the numerical simulations (Figs. 3a and 4a). The lower boundary of the active mixing zone is often characterized by an abrupt increase in ages, changing widths of age distributions, lower age–depth rates and a decrease in the bioturbated fraction. This is clearly visible in the termite study by Kristensen et al. (2015), where the fraction of saturated grains increases from 0% to 4% in the active mixing zone to up to 60% in the layers below (data not shown), accompanied by a jump in the luminescence ages and an increase in the uncertainties. The same is visible in the data from Madsen et al. (2011), who measured luminescence-based age–depth curves from aliquots collected in tidal flats, which are bioturbated by mounding lugworms. There is a clear distinction between the active mixing zone, with narrow age distributions and steeper age–depth gradients, and the underlying depositional sequence.

The age–depth curves of bioturbation by subsurface mixing display completely different characteristics (Fig. 6). The limited bleaching at the surface and the diffusion-like transport lead to a low population of bleached particles in the subsurface and wide luminescence distributions. The stochastic nature of particle transport by subsurface mixing is clearly visible in the ant dataset (Fig. 3c; Román-Sánchez et al., 2019b), with only a few luminescent grains in the subsoil that show a high age range. Ants often create mounds at their nest entrances (Richards, 2009), suggesting that luminescence-based depth profiles for ants should contain mounding signals as well. Román-Sánchez et al. (2019b) studied a profile on a hilltop with an equilibrium between soil erosion and soil production. If the erosion primarily removed the surface mounds, the subsurface mixing component of bioturbation would be amplified. The low bioturbated fraction and wide age distributions are also consistent in other luminescence datasets with considerable subsurface mixing components, e.g. root activity (Stockmann et al., 2013; Johnson et al., 2014), or at sites where material mounded by ants and wombats has been washed away by overland flow (Heimsath et al., 2002; Wackett et al., 2018). Two of these datasets only contained a small proportion of non-saturated grains (Heimsath et al., 2002; Stockmann et al., 2013). Surprisingly, the data of Johnson et al. (2014) had a very low number of saturated grains in their dataset, which they attribute to an aeolian input of bleached quartz grains. Erosion by water or soil creep can result in shallower bioturbated profiles with higher ages. The impacts on bioturbated fraction vary per process: water erosion tends to produce lower bioturbated fractions, while soil creep leads to higher bioturbated fractions (Román-Sánchez et al., 2019b). These effects are comparable to those caused by changes in bioturbation rates in

stable landscape positions. Therefore, it is important to consider the potential occurrence of erosion before interpreting luminescence–depth profiles resulting from bioturbation, as this can substantially change the interpretation. The worm and termite datasets were collected from flat terrain and were therefore not significantly impacted by erosion processes.

In addition to the studied processes, there are various other forms of bioturbation. One example is upheaval, involving the sudden detachment, homogenization and re-deposition of soil. For example, when a tree is uprooted, the soil from the root clump falls back into the pit (Gabet et al., 2003). Ploughing could also be considered upheaval. Here, a body of soil is efficiently detached, turned over and re-deposited, e.g. by a mouldboard plough (De Alba et al., 2004; Van der Meij et al., 2019). Due to its constant mixing rate with depth and homogenization of the soil, upheaval likely produces relatively homogeneous age distributions in the active mixing zone, with an abrupt increase in age below this zone. The ages, distribution widths and bioturbated fractions depend on the frequency and mixing depth of the upheaval. We expect that upheaval did not contribute to the experimental datasets used in this study, as they were sampled from sparsely forested savannah ecosystems and there are no homogeneous age distributions in the active mixing zones (Fig. 3). Bioturbation by upheaval and its interactions with mounding and subsurface mixing will be explored in future research.

The distinct effects of different bioturbation processes on soil fluxes that we identified here emphasize the necessity of including multiple formulations of bioturbation processes in soil evolution models and soil function models, as conventional diffusion-type subsurface mixing processes account for only a part of the soil mixing.

4.2 Luminescence as a tracer of soil mixing processes

Luminescence-based tracers rely on the exposure and bleaching of soil particles to daylight at the surface. Bleached particles are transported downward by various processes, where they can be used as tracers for soil mixing. As a result, luminescence primarily traces downward transport within soils (Gliganic et al., 2016). Luminescence-based age–depth profiles are predominantly influenced by mounding, because this process exposes more grains to daylight, and therefore they do not adequately represent subsurface mixing processes (Fig. 6a). The interquartile range, as a proxy for the width of the age distributions, reacts more quickly to changes in the balance of mounding and subsurface mixing (Fig. 6b). This suggests that the interquartile range might be key in distinguishing between mounding and subsurface mixing signals using luminescence-based tracers, which is still one of the main challenges when determining bioturbation rates (Wilkinson et al., 2009; Halfen and Hasiotis, 2010). This will be explored further in Sect. 4.3.

The bioturbated fraction acts as a downward tracer of soil mixing due to the supply of bleached grains from the sur-

face but can act as an upward tracer of soil mixing as well (Reimann et al., 2017). Bedrock weathering, increased bioturbation and surface denudation lead to downward migration of the active mixing zone, introducing saturated grains from the bottom up into the soil profile. These processes were not accounted for in this study. However, they do play a significant role in interactions between bioturbation and hillslope processes (Román-Sánchez et al., 2019a, b) and should be taken into account when applying bioturbation models in two- to three-dimensional settings.

The modal ages, interquartile range and bioturbated fraction are influenced not only by the types of bioturbation processes, but also by the applied depth function and process parameters such as the soil mixing rate. In Fig. 7, we have compiled an overview of how different processes, implementations and parameters affect the depth functions of luminescence-based metrics. The characteristics of these depth functions offer qualitative insights into the characteristics of the underlying mixing processes.

The majority of soil mixing happens in the active mixing zone, with the maximum depth being determined by the reach of organisms into the soil (Fig. 3), which is represented by the depth decay parameters in the simulations. This zone is distinguished from underlying layers by younger, measurable ages and a higher bioturbated fraction. It is challenging to determine the depth function of mixing processes from age–depth profiles. This supports earlier statements about determining the depth dependency of soil mixing (Gray et al., 2020). The steepness of the exponential age–depth profiles can be a result of either a different depth function or a different soil mixing rate. The dominant mixing process can be derived from the bioturbated fraction and the interquartile range, where a higher proportion of mounding results in higher bioturbated fractions and lower interquartile ranges.

The combination of luminescence-based ages, the interquartile range and the bioturbated fraction provides a comprehensive toolbox for tracing soil mixing processes. Ideally, these tracers are combined and verified with independent tracers that trace either downward or upward transport. Fallout radionuclides or meteoric cosmogenic radionuclides are examples of downward-oriented tracers (Tyler et al., 2001; Kaste et al., 2007; Johnson et al., 2014), while in situ created cosmogenic nuclides (Heimsath et al., 1997; Brown et al., 2003) and reworked clay coatings originating from Bt horizons (papules; Miedema and Slager, 1972; Sauzet et al., 2023) are produced in or below the soil column and therefore can act as upward-oriented tracers. Numerical models such as ChronoLorica provide a flexible platform to integrate different soil mixing tracers and simulate their distribution in complex multi-mixed environments.

4.3 Towards a quantitative evaluation of luminescence-based depth profiles

This qualitative understanding of the luminescence-based depth profiles, coupled with a model capable of simulating various bioturbation processes, sets the stage for quantitatively determining the impact and rates of different bioturbation processes through model calibration. Here we make a first attempt to showcase the potential of the model to derive quantitative bioturbation parameters through calibration. We do this for the termite and worm datasets, using the accompanying Mixed Signals model (see Sect. 4.4). We do not attempt a calibration for the ant dataset, because the effects of erosion and soil formation on this profile are not sufficiently constrained in the model.

For the calibration, we follow the same categories of parameters as reported in Table 1. We based the environmental parameters on field observations and experimental results. We used the same model-based parameters as reported in Table 1, with the exception of the layer thickness. This was set to 2 cm to reduce the calculation time. At this stage, the bioturbation is not grain-size-specific, so the model output is insensitive to differences in the parent material composition. Therefore, these were not modified for the calibration.

To determine the process-based parameters, we ran the model with varying depth functions, potential bioturbation rates and contributions of mounding and subsurface mixing. We determined the parameter set that produced the closest match with the experimental data by minimizing the combined squared error ($\text{error}_{\text{squared}}$) of the experimental and simulated modal ages, the interquartile range and the bioturbated fraction (Eq. 8), where P is the number of luminescence metrics and O is the number of observations in the experimental dataset.

$$\text{error}_{\text{squared}} = \sum_{p=1}^P \sum_{o=1}^O (p(o_{\text{simulated}}) - p(o_{\text{experimental}}))^2 \quad (8)$$

Calibration across all three metrics enabled us to capture the majority of the dynamics observed in the depth profiles resulting from different processes and parameters (Fig. 7). To ensure equal weighting of the three metrics, the ages were normalized by dividing them by the runtime (i.e. the bioturbation period) of the model. Consequently, all the metrics have potential values ranging from 0 to 1. Alternatively, the evaluation metric could be based on statistical tests that measure the similarity between the experimental and simulated age distributions, such as the Kolmogorov–Smirnov test or the Earth mover’s distance.

The model is well equipped to reproduce the experimental luminescence-based depth profiles (Fig. 8). The simulated depth profiles of the three metrics approach the experimental depth profiles, with some deviations due to fluctuations in the experimental data and the calibration on three different metrics. For the worm dataset, the parameter set that resulted in the lowest squared error contained a gradational depth profile, a potential bioturbation rate of $1.5 \text{ kg m}^{-2} \text{ a}^{-1}$,

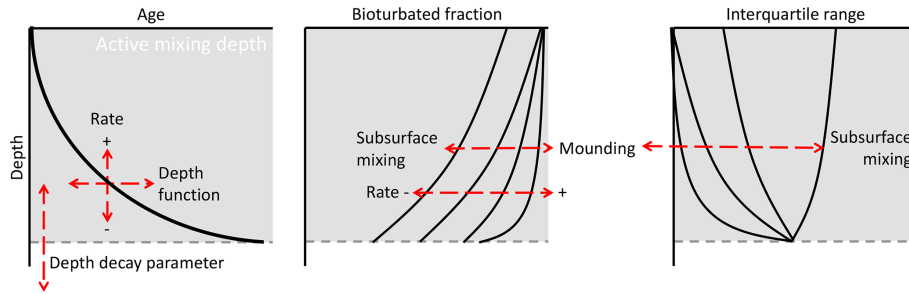


Figure 7. Conceptual overview showing how different factors and parameters affect the depth profiles of luminescence-based metrics.

90 % subsurface mixing and 10 % mounding. This ratio of processes agrees well with our expectations for burrowing anecic earthworms, which mainly live underground and sometimes visit the surface (Taylor et al., 2019). The parameter set that resulted in the lowest squared error for the termite dataset was an abrupt depth profile with a bioturbation rate of $4.5 \text{ kg m}^{-2} \text{ a}^{-1}$, 80 % subsurface mixing and 20 % mounding. We expected a much higher contribution of mounding for the termites due to their construction of large surface mounds. However, a component of subsurface mixing was also expected, as termites transport material in the subsurface when they mine material for their mounds, which is similar to subsurface galleries created by ants (Rink et al., 2013). The abrupt depth profile that was calibrated for the termite data contradicts the findings of Gray et al. (2020), who found that mixing rates generally decrease with depth.

Interestingly, the calibrated bioturbation rates are multiple orders of magnitude larger than the soil reworking rates reported in the original studies ($\sim 40 \text{ g m}^{-2} \text{ a}^{-1}$ for termites, Kristensen et al., 2015; $\sim 20\text{--}80 \text{ g m}^{-2} \text{ a}^{-1}$ for worms, von Suchodoletz et al., 2023). These reported rates were based on measured OSL ages and their depths. These ages represent the current burial ages of the grains but do not account for previous resurfacing of grains or subsurface transport without bleaching. Hence, they represent only the net displacement of soil particles from the surface to the subsurface. The calibrated rates are of the same order of magnitude as the rates of mounding and mixing determined by earthworm ingestion rates and by weighing worm casts and surface mounds (see the compilation in Wilkinson et al., 2009). Based on these factors, the actual bioturbation rates at the studied sites are probably closer to the calibrated rates than the OSL-based soil reworking rates.

This modelling exercise provides unique opportunities to quantitatively distinguish between mounding and subsurface mixing processes. However, the current results do not match our expectations, especially for the termite dataset. This discrepancy is probably a consequence of the assumption of complete bleaching within the bleaching depth in the model. The bleaching depth of 5 mm in this study was based on model estimates (Furbish et al., 2018b) and is in line with light penetration depths in rocks (0–15 mm; Meyer et

al., 2018). However, in reality, not all near-surface grains are bleached, due to the attenuation of light after it penetrates the soil surface and the formation of soil aggregates, which shield inner particles from light. Notably, the agents responsible for soil mixing are also largely responsible for soil aggregation (Lee and Foster, 1991; Bottinelli et al., 2015). A lower bleaching efficiency – the fraction of particles that is bleached within the bleaching depth – would result in lower bioturbated fractions and higher interquartile ranges, which are the same effects that a larger contribution of subsurface mixing would have.

The bleaching depth and bleaching efficiency need to be better constrained before accurate calibration of the experimental profiles is possible. These model-based parameters could be estimated through model calibration, but this comes with the risk that multiple parameter combinations could result in equally plausible mixing scenarios, as bleaching efficiency and subsurface mixing have similar effects on the calibration parameters. Experimental evidence on bleaching depths and bleaching efficiency in soils, which likely vary across soil types and vegetation cover, is thus required to constrain these parameters and provide accurate, quantitative estimates of bioturbation rates and processes based on luminescence tracers and numerical modelling.

4.4 Simulation tool for bioturbation

The simulations presented in this paper were modelled with ChronoLorica, which is a comprehensive soil-landscape evolution model that simulates multiple pedogenic and geomorphic processes, together with multiple geochronometers (Van der Meij et al., 2023). The model, without the new formulations for bioturbation, is available via the Zenodo repository (Van der Meij and Temme, 2022).

We also developed a separate model, named Mixed Signals, which contains the formulations of bioturbation processes and their effects on luminescence tracers, as described in this paper, as well as visualization and calibration tools. This model can be used or adapted for simulating bioturbation effects on luminescence-based tracers, e.g. in explorative studies or for educational purposes. The model is written in Julia, which is an interactive high-performance sci-

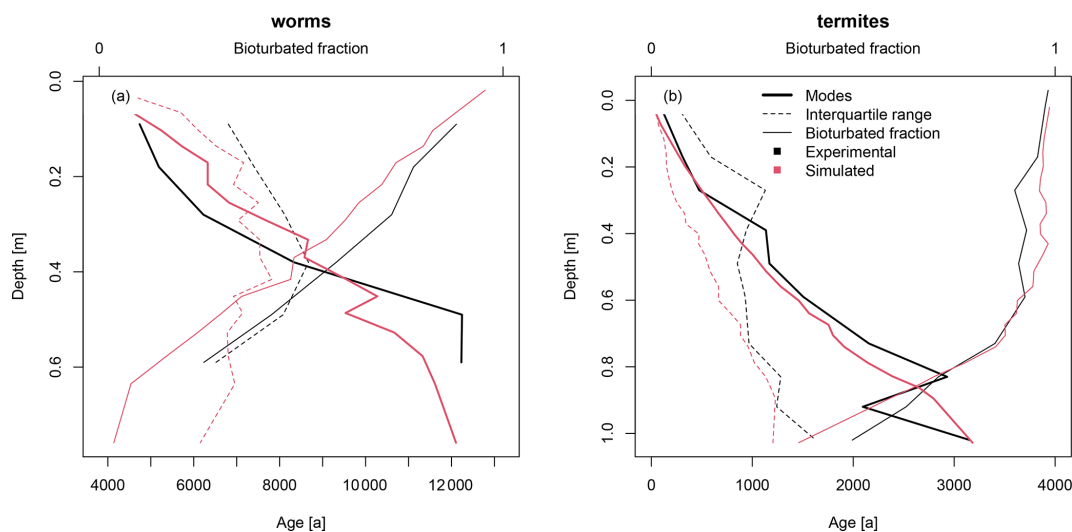


Figure 8. Calibration results for the (a) worm and (b) termite datasets. The initial layer thicknesses in the model were 2 cm. To reduce scatter in the visualization of the model results stemming from the stochastic particle transport process, the simulated results (in red) are aggregated by three layers resembling typical 5 cm thick OSL samples.

tific computing language (Bezanson et al., 2017). The Mixed Signals model is available via the Zenodo repository (Van der Meij, 2024). The download contains the following files:

- a README file with instructions to launch the model,
- a Jupyter notebook with illustrative examples demonstrating how to use the model to simulate soil mixing and its effects on luminescence-based depth profiles,
- a script with all the functions that are required to run the model and create visualizations and
- a synthetic luminescence dataset for illustrating the calibration process.

5 Conclusions

Soil bioturbation plays a crucial role in soil functions and soil evolution by cycling carbon and nutrients, but there is limited knowledge on how different mixing processes affect the fluxes and rates of soil material. In this study, we combined experimental luminescence datasets and numerical modelling to study two main bioturbation processes – mounding and subsurface mixing – and their respective mixing patterns. These mixing patterns have distinct effects on luminescence tracers, which we characterized with three metrics: the modal age of the age distribution as the most probable burial age of each layer, the interquartile range as a measure of the width of the distributions and the bioturbated fraction as the fraction of bleached particles in each layer.

By numerically simulating mounding and subsurface mixing with varying rates, depth functions and interactions between processes, we determined how each process affects the

luminescence-based depth profiles. Mounding is an advective process that moves soil material to the surface, leading to a high degree of luminescence signal resetting (bleaching), low interquartile ranges and a high bioturbated fraction. Sub-surface mixing is a diffusive process that transports a much lower number of grains from the surface, leading to high interquartile ranges and low bioturbated fractions. We summarized these effects in a conceptual diagram to facilitate qualitative interpretation of luminescence-based depth profiles.

A first attempt to quantitatively interpret luminescence-based depth profiles through model calibration showed that the model is able to reproduce the experimental depth profiles and provide realistic bioturbation rates. The model is not yet equipped to accurately determine the relative contribution of mounding and subsurface mixing in the experimental datasets, likely due to overestimating the degree of bleaching at the surface. Experimental data on bleaching depth and bleaching efficiency in soils are required before accurate, quantitative estimates of bioturbation rates and processes can be determined.

Our compilation of luminescence-based soil tracer studies and numerical simulations shows that bioturbation is more than a simple diffusive mixing process. Different organisms cause different transport processes in the soil, with major differences in fluxes of soil material and consequently nutrients and carbon. We provide numerical formulations of two main bioturbation processes, which could be used to improve soil function and soil evolution models. The accompanying Mixed Signals model contains these implementations and can be used for explorative studies, educational purposes and quantitative determination of bioturbation parameters through model calibration.

Code and data availability. The luminescence data used in this study have been published in earlier works (Kristensen et al., 2015, <https://doi.org/10.1016/j.quageo.2015.02.026>; Román-Sánchez et al., 2019b, <https://doi.org/10.1002/esp.4628>; von Suchodoletz et al., 2023, <https://doi.org/10.1038/s41598-023-32005-9>), and we refer the reader to the authors of these works for data requests. The ChronoLorica model is publicly available at <https://doi.org/10.5281/zenodo.7875033> (Van der Meij and Temme, 2022). The new bioturbation implementations can be found in the maintained version of ChronoLorica and other versions of Lorica at https://github.com/arnaudtemme/lorica_all_versions (Temme and Van der Meij, 2024) and will be added to a new version of the model. The Mixed Signals model is available at <https://doi.org/10.5281/zenodo.14603831> (Van der Meij, 2024).

Supplement. The supplement related to this article is available online at: <https://doi.org/10.5194/soil-11-51-2025-supplement>.

Author contributions. WMvdM: conceptualization, methodology, software, visualization, writing – original draft. SR: conceptualization, investigation, writing – review and editing. TR: conceptualization, writing – review and editing.

Competing interests. The contact author has declared that none of the authors has any competing interests.

Disclaimer. Publisher's note: Copernicus Publications remains neutral with regard to jurisdictional claims made in the text, published maps, institutional affiliations, or any other geographical representation in this paper. While Copernicus Publications makes every effort to include appropriate place names, the final responsibility lies with the authors.

Acknowledgements. We thank Jeppe Aagaard Kristensen (Aarhus University) and Kristina Jørkov Thomsen (Technical University of Denmark) for sharing the termite dataset, and we thank Andrea Román-Sánchez for the sample preparation and measurements of the ant dataset. We thank Hans von Suchodoletz (University of Leipzig) for collecting the samples and providing context information on the worm dataset. We are also grateful to the reviewers and editors for their valuable feedback on the manuscript.

Financial support. Svenja Riedesel acknowledges support from the European Union's Horizon Europe Marie Skłodowska-Curie Actions (RECREATE, grant no. 101103587).

This open-access publication was funded by Universität zu Köln.

Review statement. This paper was edited by Katerina Georgiou and reviewed by Shannon Mahan, Hao Long, and Adrian A Wackert.

References

- Bateman, M. D., Frederick, C. D., Jaiswal, M. K., and Singhvi, A. K.: Investigations into the potential effects of pedoturbation on luminescence dating, *Quaternary Sci. Rev.*, 22, 1169–1176, [https://doi.org/10.1016/S0277-3791\(03\)00019-2](https://doi.org/10.1016/S0277-3791(03)00019-2), 2003.
- Bateman, M. D., Boulter, C. H., Carr, A. S., Frederick, C. D., Peter, D., and Wilder, M.: Preserving the palaeoenvironmental record in Drylands: Bioturbation and its significance for luminescence-derived chronologies, *Sediment. Geol.*, 195, 5–19, <https://doi.org/10.1016/j.sedgeo.2006.07.003>, 2007.
- Bezanson, J., Edelman, A., Karpinski, S., and Shah, V. B.: Julia: A Fresh Approach to Numerical Computing, *SIAM Rev.*, 59, 65–98, <https://doi.org/10.1137/141000671>, 2017.
- Bottinelli, N., Jouquet, P., Capowiez, Y., Podwojewski, P., Grimaldi, M., and Peng, X.: Why is the influence of soil macrofauna on soil structure only considered by soil ecologists?, *Soil Till. Res.*, 146, 118–124, <https://doi.org/10.1016/j.still.2014.01.007>, 2015.
- Bouché, M. B.: Stratégies lombriciennes, *Ecol. Bull.*, 25, 122–132, 1977.
- Briones, M. J. I.: Soil fauna and soil functions: a jigsaw puzzle, *Front. Environ. Sci.*, 2, 7, <https://doi.org/10.3389/fenvs.2014.00007>, 2014.
- Brown, E. T., Colin, F., and Bourlès, D. L.: Quantitative evaluation of soil processes using in situ-produced cosmogenic nuclides, *C.R. Geosci.*, 335, 1161–1171, <https://doi.org/10.1016/j.crte.2003.10.004>, 2003.
- Creamer, R. E., Barel, J. M., Bongiorno, G., and Zwetsloot, M. J.: The life of soils: Integrating the who and how of multifunctionality, *Soil Biol. Biochem.*, 166, 108561, <https://doi.org/10.1016/j.soilbio.2022.108561>, 2022.
- De Alba, S., Lindstrom, M., Schumacher, T. E., and Malo, D. D.: Soil landscape evolution due to soil redistribution by tillage: a new conceptual model of soil catena evolution in agricultural landscapes, *CATENA*, 58, 77–100, <https://doi.org/10.1016/j.catena.2003.12.004>, 2004.
- Duller, G. A. T.: Single-grain optical dating of Quaternary sediments: why aliquot size matters in luminescence dating, *Boreas*, 37, 589–612, <https://doi.org/10.1111/j.1502-3885.2008.00051.x>, 2008.
- Furbish, D. J., Roering, J. J., Almond, P., and Doane, T. H.: Soil particle transport and mixing near a hillslope crest: 1. Particle ages and residence times, *J. Geophys. Res.-Earth*, 123, 1052–1077, <https://doi.org/10.1029/2017JF004315>, 2018a.
- Furbish, D. J., Roering, J. J., Keen-Zebert, A., Almond, P., Doane, T. H., and Schumer, R.: Soil particle transport and mixing near a hillslope crest: 2. Cosmogenic nuclide and optically stimulated luminescence tracers, *J. Geophys. Res.-Earth*, 123, 1078–1093, <https://doi.org/10.1029/2017JF004316>, 2018b.
- Gabet, E. J.: Gopher bioturbation: field evidence for non-linear hillslope diffusion, *Earth Surf. Proc. Land.*, 25, 1419–1428, [https://doi.org/10.1002/1096-9837\(200012\)25:13<1419::AID-ESP148>3.0.CO;2-1](https://doi.org/10.1002/1096-9837(200012)25:13<1419::AID-ESP148>3.0.CO;2-1), 2000.
- Gabet, E. J., Reichman, O. J., and Seabloom, E. W.: The effects of bioturbation on soil processes and sedi-

- ment transport, *Annu. Rev. Earth Pl. Sc.*, 31, 249–273, <https://doi.org/10.1146/annurev.earth.31.100901.141314>, 2003.
- Galbraith, R. F. and Roberts, R. G.: Statistical aspects of equivalent dose and error calculation and display in OSL dating: An overview and some recommendations, *Quat. Geochronol.*, 11, 1–27, <https://doi.org/10.1016/j.quageo.2012.04.020>, 2012.
- Gliganic, L. A., May, J.-H., and Cohen, T. J.: All mixed up: Using single-grain equivalent dose distributions to identify phases of pedogenic mixing on a dryland alluvial fan, *Quatern. Int.*, 362, 23–33, <https://doi.org/10.1016/j.quaint.2014.07.040>, 2015.
- Gliganic, L. A., Cohen, T. J., Slack, M., and Feathers, J. K.: Sediment mixing in aeolian sandsheets identified and quantified using single-grain optically stimulated luminescence, *Quat. Geochronol.*, 32, 53–66, <https://doi.org/10.1016/j.quageo.2015.12.006>, 2016.
- Gray, H. J., Keen-Zebert, A., Furbish, D. J., Tucker, G. E., and Mahan, S. A.: Depth-dependent soil mixing persists across climate zones, *P. Natl. Acad. Sci. USA*, 117, 8750–8756, <https://doi.org/10.1073/pnas.1914140117>, 2020.
- Halfen, A. F. and Hasiotis, S. T.: Neochronological study of the traces and burrowing behaviors of the Western harvester ant *Pogonomyrmex occidentalis* (insecta: Hymenoptera: Formicidae): paleopedogenic and paleoecological implications, *PALAIOS*, 25, 703–720, <https://doi.org/10.2110/palo.2010.p10-005r>, 2010.
- Hanson, P. R., Mason, J. A., Jacobs, P. M., and Young, A. R.: Evidence for bioturbation of luminescence signals in eolian sand on upland ridgetops, southeastern Minnesota, USA, *Quatern. Int.*, 362, 108–115, <https://doi.org/10.1016/j.quaint.2014.06.039>, 2015.
- Heimsath, A. M., Dietrich, W. E., Nishiizumi, K., and Finkel, R. C.: The soil production function and landscape equilibrium, *Nature*, 388, 358–361, <https://doi.org/10.1038/41056>, 1997.
- Heimsath, A. M., Chappell, J., Spooner, N. A., and Questiaux, D. G.: Creeping soil, *Geology*, 30, 111–114, [https://doi.org/10.1130/0091-7613\(2002\)030<0111:CS>2.0.CO;2](https://doi.org/10.1130/0091-7613(2002)030<0111:CS>2.0.CO;2), 2002.
- Johnson, M. O., Mudd, S. M., Pillans, B., Spooner, N. A., Keith Fifield, L., Kirkby, M. J., and Gloor, M.: Quantifying the rate and depth dependence of bioturbation based on optically-stimulated luminescence (OSL) dates and meteoric ^{10}Be , *Earth Surf. Proc. Land.*, 39, 1188–1196, <https://doi.org/10.1002/esp.3520>, 2014.
- Kaste, J. M., Heimsath, A. M., and Bostick, B. C.: Short-term soil mixing quantified with fallout radionuclides, *Geology*, 35, 243–246, <https://doi.org/10.1130/G23355A.1>, 2007.
- Kraus, D., Brandl, R., Achilles, S., Bendix, J., Grigusova, P., Larsen, A., Plischoff, P., Übernickel, K., and Farwig, N.: Vegetation and vertebrate abundance as drivers of bioturbation patterns along a climate gradient, *PLoS ONE*, 17, e0264408, <https://doi.org/10.1371/journal.pone.0264408>, 2022.
- Kristensen, J. A., Thomsen, K., Murray, A., Buylaert, J.-P., Jain, M., and Breuning-Madsen, H.: Quantification of termite bioturbation in a savannah ecosystem: Application of OSL dating, *Quat. Geochronol.*, 30, 334–341, <https://doi.org/10.1016/j.quageo.2015.02.026>, 2015.
- Lee, K. E. and Foster, R. C.: Soil fauna and soil structure, *Soil Res.*, 29, 745–775, <https://doi.org/10.1071/sr9910745>, 1991.
- Madsen, A. T., Murray, A. S., Jain, M., Andersen, T. J., and Pejrup, M.: A new method for measuring bioturbation rates in sandy tidal flat sediments based on luminescence dating, *Estuar. Coast. Shelf* S., 92, 464–471, <https://doi.org/10.1016/j.ecss.2011.02.004>, 2011.
- Meng, X., Kooijman, A. M., Temme, A. J. A. M., and Cammeraat, E. L. H.: The current and future role of biota in soil-landscape evolution models, *Earth-Sci. Rev.*, 103945, <https://doi.org/10.1016/j.earscirev.2022.103945>, 2022.
- Meyer, M. C., Gliganic, L. A., Jain, M., Sohbati, R., and Schmidmair, D.: Lithological controls on light penetration into rock surfaces – Implications for OSL and IRSL surface exposure dating, *Radiat. Meas.*, 120, 298–304, <https://doi.org/10.1016/j.radmeas.2018.03.004>, 2018.
- Michel, E., Néel, M.-C., Capowicz, Y., Sammartino, S., Lafolie, F., Renault, P., and Pelosi, C.: Making Waves: Modeling bioturbation in soils – are we burrowing in the right direction?, *Water Res.*, 216, 118342, <https://doi.org/10.1016/j.watres.2022.118342>, 2022.
- Miedema, R. and Slager, S.: Micromorphological Quantification of Clay Illuviation, *J. Soil Sci.*, 23, 309–314, <https://doi.org/10.1111/j.1365-2389.1972.tb01662.x>, 1972.
- Minasny, B., Stockmann, U., Hartemink, A. E., and McBratney, A. B.: Measuring and Modelling Soil Depth Functions, in: *Digital Soil Morphometrics*, edited by: Hartemink, A. E. and Minasny, B., Springer International Publishing, Cham, 225–240, https://doi.org/10.1007/978-3-319-28295-4_14, 2016.
- Reimann, T., Román-Sánchez, A., Vanwalleghem, T., and Wallinga, J.: Getting a grip on soil reworking – Single-grain feldspar luminescence as a novel tool to quantify soil reworking rates, *Quat. Geochronol.*, 42, 1–14, <https://doi.org/10.1016/j.quageo.2017.07.002>, 2017.
- Richards, P.: Aphaenogaster ants as bioturbators: Impacts on soil and slope processes, *Earth-Sci. Rev.*, 96, 92–106, <https://doi.org/10.1016/j.earscirev.2009.06.004>, 2009.
- Rink, W. J., Dunbar, J. S., Tschinkel, W. R., Kwapich, C., Repp, A., Stanton, W., and Thulman, D. K.: Subterranean transport and deposition of quartz by ants in sandy sites relevant to age overestimation in optical luminescence dating, *J. Archaeol. Sci.*, 40, 2217–2226, <https://doi.org/10.1016/j.jas.2012.11.006>, 2013.
- Román-Sánchez, A., Laguna, A., Reimann, T., Giraldez, J., Peña, A., and Vanwalleghem, T.: Bioturbation and erosion rates along the soil-hillslope conveyor belt, part 2: Quantification using an analytical solution of the diffusion-advection equation, *Earth Surf. Proc. Land.*, 44, 2066–2080, <https://doi.org/10.1002/esp.4626>, 2019a.
- Román-Sánchez, A., Reimann, T., Wallinga, J., and Vanwalleghem, T.: Bioturbation and erosion rates along the soil-hillslope conveyor belt, part 1: Insights from single-grain feldspar luminescence, *Earth Surf. Proc. Land.*, 44, 2051–2065, <https://doi.org/10.1002/esp.4628>, 2019b.
- Ruiz, S., Or, D., and Schymanski, S. J.: Soil Penetration by Earthworms and Plant Roots–Mechanical Energetics of Bioturbation of Compacted Soils, *PLoS ONE*, 10, e0128914, <https://doi.org/10.1371/journal.pone.0128914>, 2015.
- Sauzet, O., Cammas, C., Gilliot, J., and Montagne, D.: Long-term quantification of the intensity of clay-sized particles transfers due to earthworm bioturbation and eluviation/illuviation in a cultivated Luvisol, *Geoderma*, 429, 116251, <https://doi.org/10.1016/j.geoderma.2022.116251>, 2023.
- Schiffers, K., Teal, L. R., Travis, J. M. J., and Solan, M.: An Open Source Simulation Model for Soil

- and Sediment Bioturbation, *PLoS ONE*, 6, e28028, <https://doi.org/10.1371/journal.pone.0028028>, 2011.
- Sheather, S. J. and Jones, M. C.: A Reliable Data-Based Bandwidth Selection Method for Kernel Density Estimation, *J. Roy. Stat. Soc. B Met.*, 53, 683–690, <https://doi.org/10.1111/j.2517-6161.1991.tb01857.x>, 1991.
- Stewart, A. D. and Anand, R. R.: Anomalies in insect nest structures at the Garden Well gold deposit: Investigation of mound-forming termites, subterranean termites and ants, *J. Geochem. Explor.*, 140, 77–86, <https://doi.org/10.1016/j.gexplo.2014.02.011>, 2014.
- Stockmann, U., Minasny, B., Pietsch, T. J., and McBratney, A. B.: Quantifying processes of pedogenesis using optically stimulated luminescence, *Eur. J. Soil Sci.*, 64, 145–160, <https://doi.org/10.1111/ejss.12012>, 2013.
- Taylor, A. R., Lenoir, L., Vegerfors, B., and Persson, T.: Ant and Earthworm Bioturbation in Cold-Temperate Ecosystems, *Ecosystems*, 22, 981–994, <https://doi.org/10.1007/s10021-018-0317-2>, 2019.
- Temme, A. J. A. M. and Van der Meij, W. M.: *lorica_all_versions*, GitHub [code], https://github.com/arnaudtemme/lorica_all_versions, last access: 11 September 2024.
- Temme, A. J. A. M. and Vanwallegem, T.: LORICA – A new model for linking landscape and soil profile evolution: development and sensitivity analysis, *Comput. Geosci.*, 90, 131–143, <https://doi.org/10.1016/j.cageo.2015.08.004>, 2016.
- Tyler, A. N., Carter, S., Davidson, D. A., Long, D. J., and Tipping, R.: The extent and significance of bioturbation on ^{137}Cs distributions in upland soils, *CATENA*, 43, 81–99, [https://doi.org/10.1016/S0341-8162\(00\)00127-2](https://doi.org/10.1016/S0341-8162(00)00127-2), 2001.
- Van der Meij, W. M.: Mixed Signals - soil bioturbation simulation tool, Version v1.0, Zenodo [code], <https://doi.org/10.5281/zenodo.14603831>, 2024.
- Van der Meij, W. M. and Temme, A. J. A. M.: ChronoLorica v1.0, Zenodo [code], <https://doi.org/10.5281/zenodo.7875033>, 2022.
- Van der Meij, W. M., Reimann, T., Vornehm, V. K., Temme, A. J. A. M., Wallinga, J., van Beek, R., and Sommer, M.: Reconstructing rates and patterns of colluvial soil redistribution in agrarian (hummocky) landscapes, *Earth Surf. Proc. Land.*, 44, 2408–2422, <https://doi.org/10.1002/esp.4671>, 2019.
- Van der Meij, W. M., Temme, A. J. A. M., Wallinga, J., and Sommer, M.: Modeling soil and landscape evolution – the effect of rainfall and land-use change on soil and landscape patterns, *SOIL*, 6, 337–358, <https://doi.org/10.5194/soil-6-337-2020>, 2020.
- Van der Meij, W. M., Temme, A. J. A. M., Binnie, S. A., and Reimann, T.: ChronoLorica: introduction of a soil–landscape evolution model combined with geochronometers, *Geochronology*, 5, 241–261, <https://doi.org/10.5194/gchron-5-241-2023>, 2023.
- von Suchodoletz, H., Kühn, P., Wiedner, K., and Reimann, T.: Deciphering timing and rates of Central German Chernozem/Phaeozem formation through high resolution single-grain luminescence dating, *Scientific Reports*, 13, 4769, <https://doi.org/10.1038/s41598-023-32005-9>, 2023.
- Wackett, A. A., Yoo, K., Amundson, R., Heimsath, A. M., and Jelinski, N. A.: Climate controls on coupled processes of chemical weathering, bioturbation, and sediment transport across hillslopes, *Earth Surf. Proc. Land.*, 43, 1575–1590, <https://doi.org/10.1002/esp.4337>, 2018.
- Wilkinson, M. T., Richards, P. J., and Humphreys, G. S.: Breaking ground: Pedological, geological, and ecological implications of soil bioturbation, *Earth-Sci. Rev.*, 97, 257–272, <https://doi.org/10.1016/j.earscirev.2009.09.005>, 2009.
- Wintle, A. G. and Murray, A. S.: A review of quartz optically stimulated luminescence characteristics and their relevance in single-aliquot regeneration dating protocols, *Radiat. Meas.*, 41, 369–391, <https://doi.org/10.1016/j.radmeas.2005.11.001>, 2006.
- Yates, L. A., Aandahl, Z., Brook, B. W., Jacobs, Z., Li, B., David, B., and Roberts, R. G.: A new OSL dose model to account for post-depositional mixing of sediments, *Quat. Geochronol.*, 101502, <https://doi.org/10.1016/j.quageo.2024.101502>, 2024.
- Zhang, A., Long, H., Yang, F., Zhang, J., Peng, J., Shi, Y., and Zhang, G.: Reconstructing Mollisol Formation Processes Through Quantified Pedoturbation, *Geophys. Res. Lett.*, 51, e2024GL108189, <https://doi.org/10.1029/2024GL108189>, 2024.